Veterinary Ophthalmology (2010) **13**, 6, 369–376

Cellular-resolution *in vivo* imaging of the feline retina using adaptive optics: preliminary results

Serge G. Rosolen,*,†,‡,§ Barbara Lamory,¶ Fabrice Harms,¶ José-Alain Sahel,†,‡,§,** Serge Picaud†,‡,§ and Jean-François LeGargasson†,‡,††

**Clinique Veterinaire Voltaire, 119 Boulevard Voltaire, 92600 Asnières, France; †Inserm, UMR-S968/Institut de la Vision, 17 rue Moreau 75012 Paris, France; ‡Université Pierre et Marie Curie Paris-6, 4 place Jussieu, 75252 Paris, France; §Fondation Ophtalmologique A. de Rothshild, 25/29 rue Manin 75019 Paris, France; ¶Imagine Eyes, 18 rue Charles de Gaulle 91400 Orsay, France; **Centre Hospitalier National d'Ophtalmologie des Quinze-Vingts, 28 rue de Charenton 75571 Paris, France; and ††UDD Paris 7, 4 rue Ambroise Paré 75010 Paris, France*

Address communications to:

S. G. Rosolen

Tel.: +33 1 47 33 08 95
Fax: +33 1 47 33 30 37
e-mail: sg.rosolen@orange.fr

Abstract

Purpose To perform cellular-level *in vivo* imaging of the feline retina using an adaptive optics flood illumination fundus camera (AO FIFC) designed for the human eye.

Materials and methods Cellular-level images were obtained from three eyes of two normal sedated cats. Ocular aberrations were corrected using an AO system based on a 52-acuator electromagnetic deformable mirror and a 1024 lenslet Hartmann–Shack sensor (both Imagine Eyes, Orsay, France). A square 3°×3° area of the ocular fundus was flood-illuminated by a pulsed LED emitting at 850 nm and imaged onto a low-noise, high-resolution CCD camera. The animal's pupils were dilated and the effective pupil size was set to 7.5 mm. Conjunctival atraumatic clips were used to avoid eyeball movements and eyelid closure. The cornea was artificially hydrated throughout the experiments. Each acquisition consisted of 20 consecutive images, out of which 10 were numerically averaged to produce an enhanced final image.

Results The total amount of ocular aberrations was greatly reduced by the AO correction, from 2.4 to 0.21 microns root mean square on average. The resulting images presented white dots distributed at a density similar to that of cone photoreceptors and they allowed us to visualize small blood vessels and nerve fiber bundles at a higher resolution than classically obtained with conventional fundus photography.

Conclusion Retinal imaging with cellular resolution was feasible in cats under sedation using an AO FIFC designed for human eyes without any optical modification. The AO FIFC technology could find new applications in clinical, pharmacological, and toxicological investigations.

Key Words: adaptive optics, blood vessel, cellular resolution, cones, nerve fiber, retina

INTRODUCTION

High-resolution retinal imaging is having an increasing contribution in our understanding of physio-pathological processes underlying retinal vascular and neurologic diseases in humans[1–4] and in animals.[5–8] Fundus photography has proved to be invaluable in the documentation of posterior segment diseases among animals and direct digital acquisition of images using an electronic camera offers several advantages over conventional photography. Optical coherence tomography (OCT) is an interferometric imaging technique that can obtain micro-resolution cross-sectional, volumetric, or tomographic images of the eye. OCT is analogous to B-mode ultrasonography using photonic tissue reflectivity rather than acoustic tissue reflectivity. OCT uses short pulses of coherent light to image with a high axial resolution of 4–5 μm and a lateral resolution of 15–20 μm. For all these devices, the lateral resolution (the smallest dimension observable on the retinal plan) is limited to 20 μm meaning that retinal structures such as photoreceptors or capillaries with dimensions of only a few microns (μm) cannot be visualized. This limited optical resolution is not due to shortcomings in instrumentation but to inherent optical defects found in every eye.

Cellular-level retinal imaging is based on the ability to observe the retinal tissue by means of increased optical resolution. Retinal images in human and animal eyes are degraded by optics of the observed eye. In every eye, irregu-

lar optical defects are present and limit the optical resolution of imaging systems. These optical defects include myopia, hyperopia, and astigmatism as well as higher-order aberrations such as coma and trefoil.[9,10] The visual impact of myopia, hyperopia, and astigmatism is generally important and can be corrected with the use of glasses, contact lenses, or refractive surgery. However the quality of vision, especially with large pupil diameters, can also be decreased by higher-order aberrations (e.g. coma, trefoil, etc.).[11] These aberrations are mainly due to the optical imperfections such as surface and media irregularities, tilts or misalignments in the eye's optical components (e.g. tear film, cornea, lens, etc.). Like traditional spherical (myopia/hyperopia) and astigmatic refractive errors, these higher-order aberrations significantly impair retinal image quality.[12]

Recent theoretical and technological advances have enabled researchers to measure and correct most of these aberrations. Adaptive optics (AO) technology[13] was first used in astrophysics to improve the image quality obtained using terrestrial telescopes. The light from a star is distorted when passing through the turbulence of the atmosphere and collected by an earth-based telescope. Briefly, the principle of AO consists of measuring the optical aberrations with a sensor, calculating the optical compensation, and then changing the shape of a deformable mirror which lies in the optical path.

A Hartmann–Shack (HS) sensor is used to measure eyes' aberrations by analyzing the light of an infrared beam focused on the retina and reflected out of the eye. It has been shown that using a HS device (decomposition of a pupil in small pupils) enables a fast, precise and objective measurement of eye aberrations.[14] The HS sensor is the most commonly used technique to measure optical aberrations in currently available clinical aberrometers.[15] Aberration measurements with HS technology have been performed in monkeys,[16] mice,[17] birds,[18] and in cats and dogs.[19–21] Once the optical aberrations are measured, a deformable mirror technology[22,23] is used to compensate these aberrations measured with the HS sensor.[11,24] Figure 1 summarizes the principle of the adaptive-optics loop used in this work.

The aim of this study was to determine whether the images of the cat retina can be obtained with cellular-level resolution, using an adaptive optics flood illumination fundus camera (AO FIFC) designed for the human eye.

MATERIALS AND METHODS

The protocol adhered to the Association for Research in Vision and Ophthalmology Statement for the Use of Animals in Ophthalmic and Vision Research.

Animals

Data were obtained from three eyes of two normal, sedated domestic shorthair cats (3 and 4 years old). Both animals were found to be in good physical condition and without any visual defect following a complete clinical examination. A complete ophthalmologic examination, including slit-lamp and indirect ophthalmoscopy, was performed before

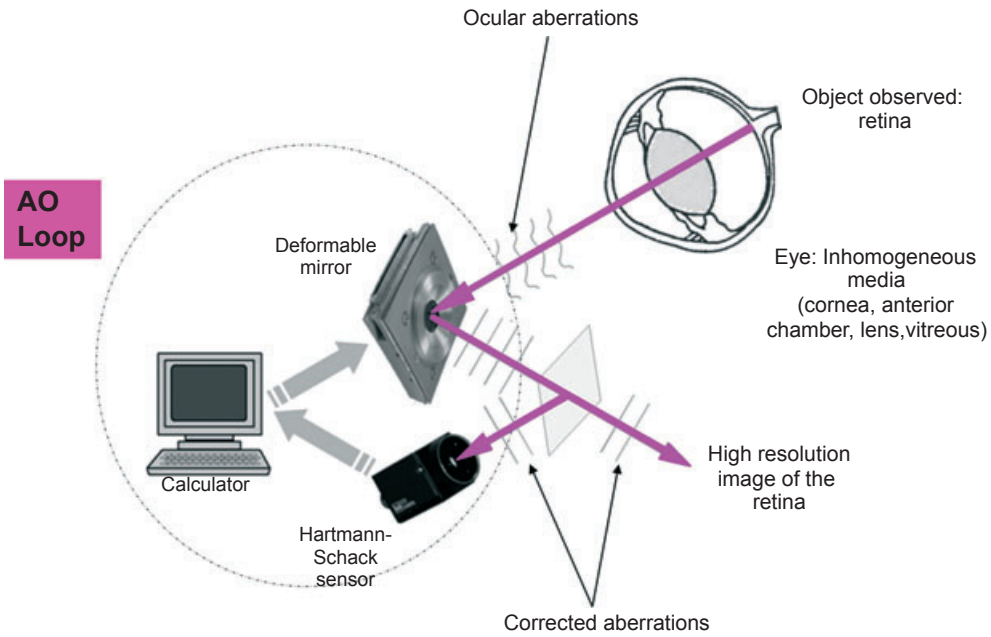

Figure 1. Schematic diagram of the adaptive-optics loop: the retina is observed throughout inhomogeneous media (cornea, anterior and posterior chambers, lens and vitreous) which induce ocular aberrations. Among those aberrations, higher orders aberrations cannot be corrected with any additional optical device such as contact lenses or glasses. At the front of the adaptive optics system (AO), a deformable mirror is used to correct those higher orders aberrations. The corrections performed by the deformable mirror are analyzed using a Hartmann–Shack (HS) sensor which enables us to obtain high-resolution images at the rear of the AO.

testing and did not reveal any signs of ocular abnormality. In addition, a fundus image was obtained thanks to a color video digital fundus camera previously described.[25,26]

Prior to sedation, the pupils were dilated using 1% tropicamide (Mydriaticum®, Théa, Rueil, France) in order to obtain a stable mydriasis of at least 7.5 mm in diameter over the entire assessment session. The animals were sedated with a single intramuscular injection of medetomidine (0.1 mg/kg, Domitor®; Pfizer, Orsay, France). The cornea was topically anesthetized with two drops of tetracaine 1% (Tetracaine; Novartis, Rueil, France). The eye fixation was performed with the use of a conjunctival atraumatic clip positioned at 12 o'clock as previously described (Fig. 2a,b).[27] The clip was also used to move the eye in various directions according to three different axes. Once the eye was positioned in the appropriate position, the clip's fixation was finalized with the help of an adjustable head contention device as described previously.[28] The corneal hydration was performed by regular instillation of eye drops (BSS, Alcon, Rueil-Malmaison, France).

Adaptive optics and image analysis

The distance between the eye's pupil plan and the front of the machine was approximately 5 cm (Fig. 2c). The cat's pupil was displayed on the screen of the computer and the distance adjustment was performed manually. Ocular aberrations were measured and corrected using an AO system operating in a closed-loop configuration at 10 Hz, based on a 52-acuator electromagnetic deformable mirror and a 1024 lenslet HS sensor (both from Imagine Eyes). Then, we adjusted the focus of the system to image the different layers in the retina. The focus could be changed by up to 300 μm onto the retina. The lateral resolution of the system was approximately 3 μm and the axial resolution of the system was 40 μm. A 3° × 3° square area of the fundus was flood-illuminated by a pulsed LED emitting at 850 nm and imaged onto a low-noise, high-resolution CCD camera (Roper Scientific, Tucson, AZ, USA). To avoid image saturation due to the reflection of the tapetum lucidum, the optimal exposure time was set to 3 ms. Each acquisition consisted of 20 consecutive images, out of which, 10 were numerically averaged to produce an enhanced final image. The entire procedure lasted approximately 20 min. Image calibration was achieved by the AO apparatus based on cat's axial length values given by the literature (*c.* 21.30 mm).[29]

Afterwards, images were localized manually with the help of those obtained with a color video fundus camera (AIDA Storz, 38 mm, Rueil-Malmaison, France) equipped with a 2.7-mm probe (Storz, Rueil-Malmaison, France) as previously described.[26]

RESULTS

For the measurement, the effective pupil size was that of our optical system (7.5 mm) whereas the animal dilated pupil often exceeded the sensor area. The average total amount of ocular aberrations, excluding sphere, was 2.4 ± 1.0 μm root mean square (RMS) (Table 1). Sphere aberration (myopia/hyperopia) was compensated by an optical Badal system that changes the focus without changing the optical field. For all examined eyes, the total amount of ocular aberrations was strongly reduced by the AO correction to an average spatial residual error of 0.21 ± 0.03 μm RMS (Table 1). These data could be compared with the data obtained with the same device in human eyes. For 36 healthy human eyes, the residual error after AO correction was 0.14 ± 0.05 μm whereas the total amount of ocular aberrations was 1.36 ± 1.25 μm.[30] The image acquisition time was reduced in comparison to that used on humans.

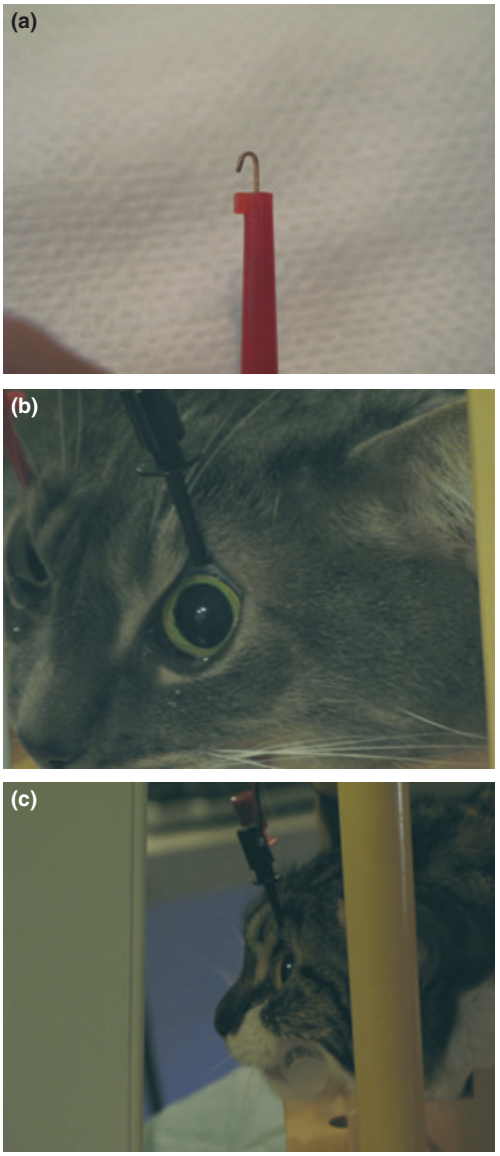

Figure 2. Adaptive optics in cat: the cat is positioned in sternal recumbancy, the eye is fixed with the help of an atraumatic retractable copper clip (a), positioned at the conjunctiva (b). The head is positioned at 5 cm from the AO device (c).

Table 1. Individual values of optical aberration measurements before and after correction by AO in cat and humans. In humans, pupil dilation was obtained by instillation of drops of tropicamide (0.5%), a chinrest was used to stabilize the head of the subject and an internal fixation target enabled the user to image the desired area of the retina. The subject had to blink before each acquisition. For each eye the root mean square (RMS), total amount of ocular aberrations (except sphere) was the first measurement made before AO correction. RMS residual errors are spatial standard deviations of wavefront obtained after AO correction (mean was obtained by averaging 100 measurements/eye). These data indicated that the correction was correct and stable during the experiment. Values given for humans were obtained from Ref. 30

Animal	Observed eye	Pupil size (mm)	RMS ocular aberrations (except sphere) (μm)	RMS residual error (μm) (mean ± SD)
Cat 1	OD	9.9	3.6	0.22 ± 0.10
Cat 2	OD	10.3	1.8	0.24 ± 0.07
Cat 2	OS	9.6	1.7	0.18 ± 0.02
Humans (n = 36)	OS	7.6 ± 0.7	1.36 ± 1.25	0.14 ± 0.05

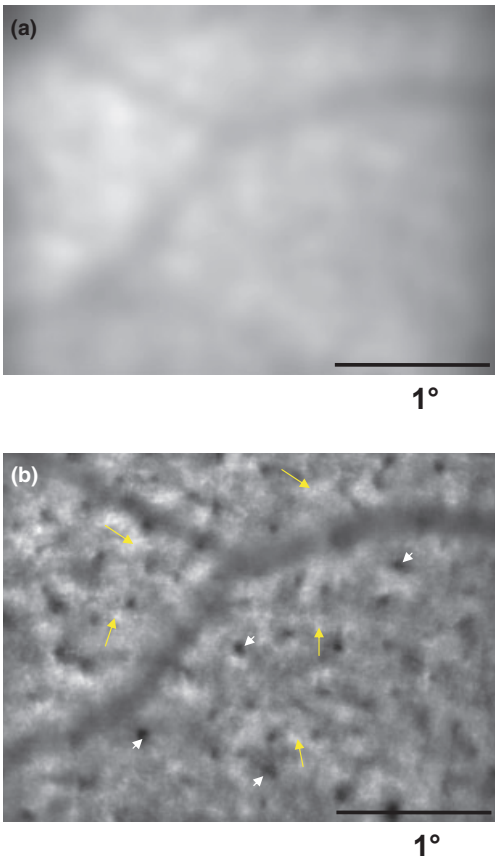

Figure 3. Retinal images of the right eye of cat 1 (a) before correction by the AO system and (b) after correction and averaging of 10 frames. The correction made by the AO system enhances the contrast and spatial resolution of the image at exactly the same position. These corrections and averaging of the image enables us to visualize elements such as white dots (arrows) and black clusters (arrowheads). Horizontal bar calibration = 1° (1° represents 300 μm).

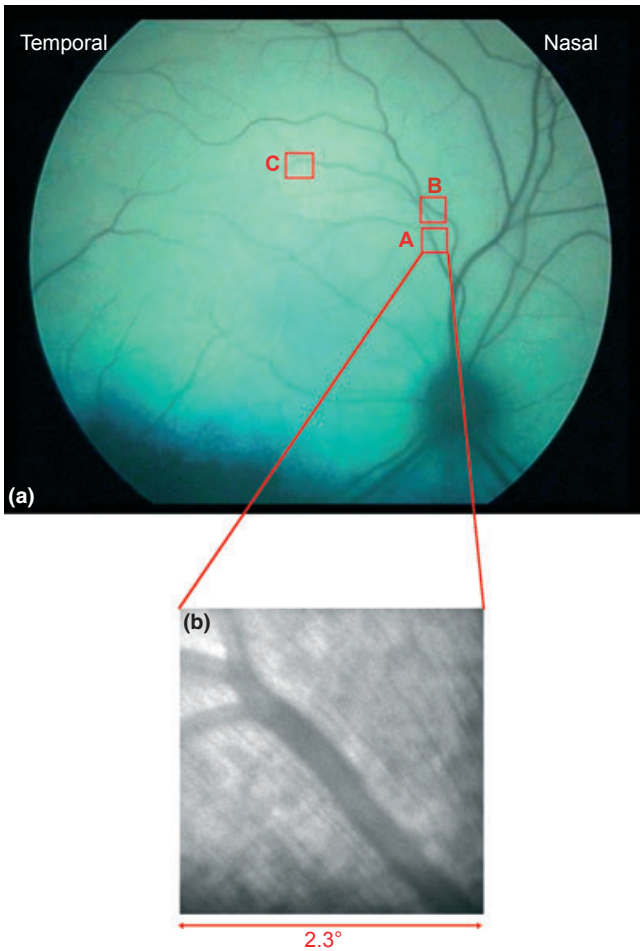

Figure 4. High-resolution image of the cat retina: The fundus ophthalmoscopy (vessel morphology) of the right eye of cat 1 (Fig. 4a) was used to locate the areas (A, B, C) previously imaged by adaptive optics AO image of the area A obtained after correction and averaging of 10 frames is illustrated in Fig. 4b. Calibration is expressed in degree. 1° degree represents 300 μm.

Figure 3 illustrates retinal images before (Fig. 3a) and after (Fig. 3b) correction by the AO system. In fact, Fig. 3a corresponds to the image that would be obtained with a conventional eye fundus camera. The correction made by the AO system in Fig. 3b enhances the contrast and spatial resolution of the image at exactly the same position. These corrections and averaging of the image enables us to visualize elements such as white dots (arrows) and black clusters (arrowheads). These AO images can be correlated to their retinal positions on fundus images using anatomical markers like blood vessels. Figure 4 illustrates the strategy followed

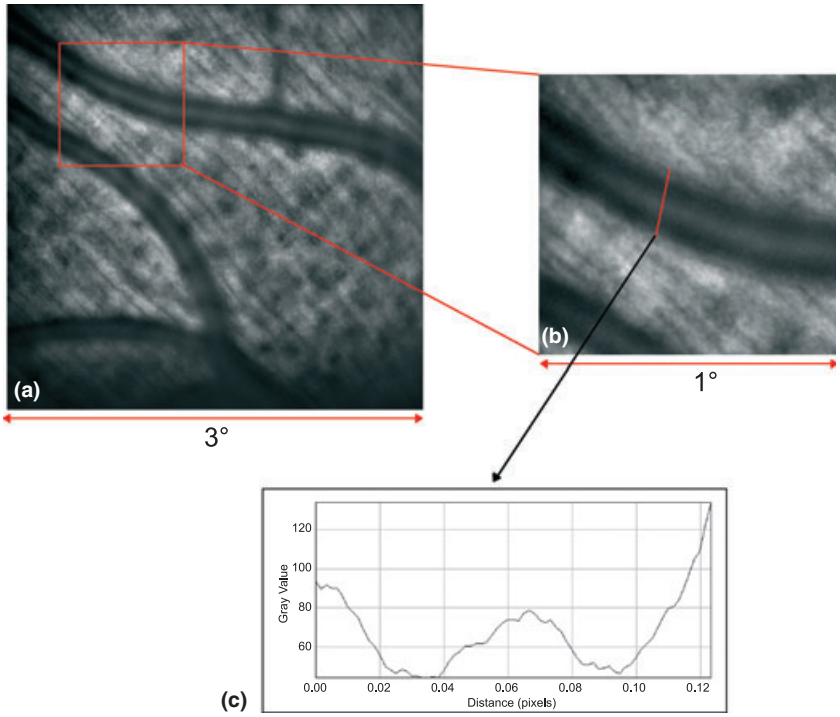

Figure 5. High-resolution image of blood vessels of the cat retina. These images were obtained from the area located in inset B of Fig. 4a. The red square in (a) was further magnified in (b) to show the blood vessel profile. Its gray value is provided in (c) showing a 30 μm diameter.

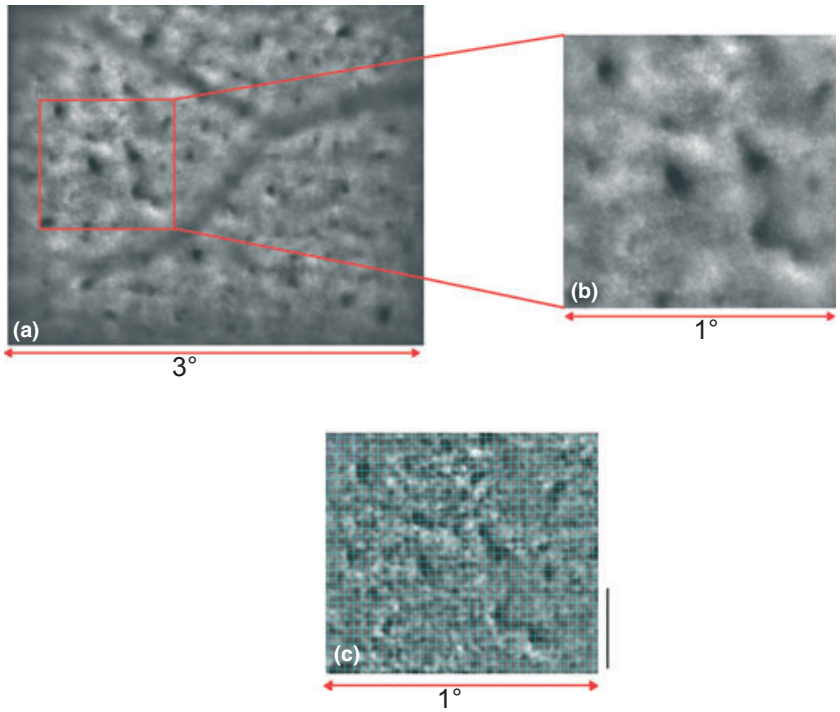

Figure 6. High-resolution images obtained in an area located above the area centralis at the superior temporal midperiphery (inset C in Fig. 4a): a part (red square) of the image (a) was enlarged (b) to better visualize retinal details. White dots were visible on these enlarged AO images (c). Using ImageJ software, the AO images were processed to enhance the contrast of white dots and to evaluate their density into the retina. The power spectrum of the image was used to obtain the white dots frequencies and then we performed a band pass filter to keep only these frequencies in the image. The image's dynamic was improved by stretching the grayscale histogram. White dot counting was made using a grid in which the basic elements correspond to 10×10 μm. Their density was thus estimated on the image [density: 7000 cells/mm^2 (*c.* 70 cells in 0.01 mm^2)]. The vertical bar represents 100 μm.

to locate the AO image positions on the right eye fundus of cat 1.Vessel morphology was used to identify the examined areas (inset A, inset B, inset C) and to locate the corresponding position on the previously performed fundus ophthalmoscopy (Fig. 4a). AO image of the area A (inset A) is illustrated in Fig. 4b. AO image of area B (inset B) is illustrated in Fig. 5a and AO image of area C (inset C) is illustrated in Fig. 6a. Note on AO images that blood vessels could be seen with high resolution as shown in Fig. 5a,b. Plot profile obtained (Fig. 5c) with an image analysis soft-

ware (IMAGEJ 1.41 freeware) enabled us to clearly define the vessel diameter (30 μm). On enlarged AO images (Figs 4b,5a), from areas located in inset A and inset B of the Fig. 4a, images at the nerve fiber layer clearly showed individual axon bundles running in parallel toward the optic nerve. These images were similar to those obtained with the same device in the human eyes although axon bundles were more visible in the cat retina than previously described in humans.[30] On enlarged AO images obtained in areas located above the area centralis at the superior temporal midperiphery, white dots were clearly visible (Fig. 6b,c) in the three different examined eyes. The white dot density was then counted with the image analysis software, IMAGEJ 1.41 freeware (see legend of Fig. 6). This density was estimated at 6984 ± 97 cells/mm^2 (n = 3, SEM). When images were acquired in the more central area (close to area centralis) white dots were not clearly detectable (see Discussion for interpretation). In addition, some black clusters were visible in the cat (Figs 3b,6) retinal images, similar to those sometimes observed in the human retina,[30] but bigger in size and number.

Figure 7 illustrates images obtained in different layers of the cat's retina (left eye of cat 2). Similar to those observed in Fig. 3a for cat 1, the black clusters seen in the Fig. 7a were less visible when imaging at approximately the same location 10 min later (Fig. 7b) and not visible in the nerve fiber layer (Fig. 7c). When visible, the location of these black points remained exactly identical between different series of images as demonstrated by superimposition of the red tracing.

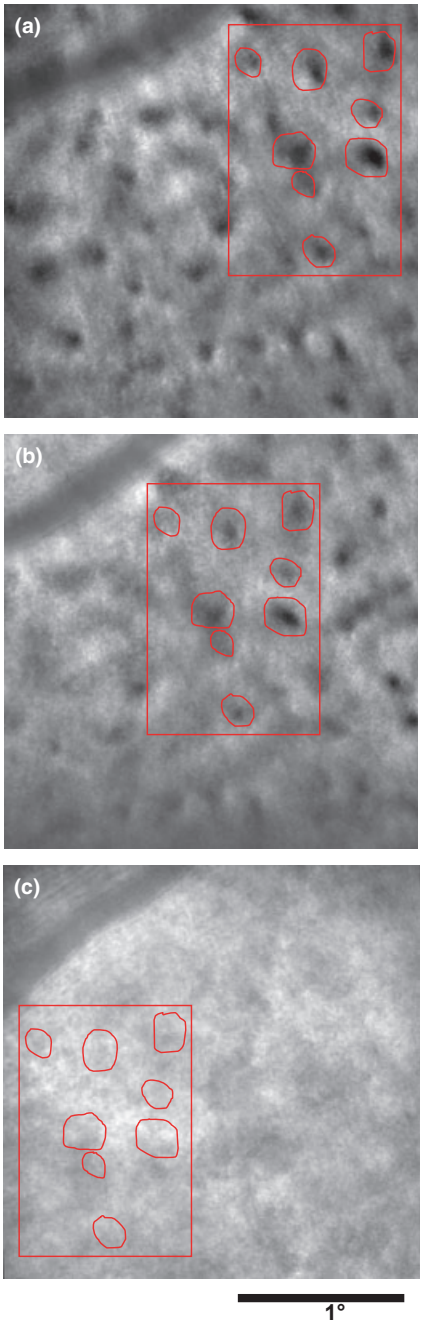

Figure 7. Images obtained in the left eye of cat 2 for different depths: at the presumed level of photoreceptors (a), then 10 min later at approximately the same location (b), and at the level of nerve fiber layer (c). By autocorrelation analysis dark clusters were found at exactly the same locations in (a) and (b) but they were not visible at the level of the nerve fiber layer.

DISCUSSION

When AO images were generated in cats, white dots were visible. These white dots were highly reminiscent of those observed in the human retina and attributed to cone photoreceptors. The estimation of their density in an area located in the superior temporal midperiphery (6984 cell/mm^2) is consistent with the cone density (5000–8000 cells/mm^2) described in this area in the cat retina.[31,32] Furthermore, white dots were not clearly detectable in the area closer to the cat area centralis, similarly cones are not clearly detectable in the human fovea. Indeed, the current AO resolution and the smaller foveal cone size do not allow their visualization. This resolution limitation may also apply to cones in the cat area centralis. Therefore, these similarities with the human cone images and with the cat cone densities suggest that these white dots probably correspond to cone photoreceptors.

Despite the fact that higher-order aberrations are relatively larger in carnivores when compared with those in the human eye,[33,34] optical aberrations measured in cats did not impede us from using an AO system designed for the human eye without any additional optical change. Animal models have long been used in ocular research but it has been difficult to quantify their ocular aberrations because accurate measurement of these aberrations requires normal corneal physiology and in particular, adequate hydration. A normal, uniform tear film needs to be maintained while the measurements are taken, otherwise significant changes in aberrations occur.[35] Anesthesia seriously compromises the quality and the quantity of the tear film as these animals are no longer able to blink. Some anesthetic combinations increase the corneal dehydration,[36,37] so measurement reproducibility can be improved by corneal hydration.

To image human eyes, the patient has to fix on a target in order to help the ophthalmologist to achieve a specific eccentricity. In animals, fixation of the eye is necessary but that fixation must often be done atraumatically in order to perform examinations. Our system enabled us to move the globe in all directions, then to maintain the appropriate fixed position throughout the examination. This is an important point to perform reproducible examinations.

Using AO, images of blood vessel walls were visualized thus representing a useful tool for studying microcirculation. Nerve fiber bundles could be easily identified. In addition, in feline eyes, RMS residual error values after AO corrections were higher than those measured in human eyes thus inducing a lower optical resolution. This could explain why details were less visible in feline eyes without the use of any additional optical device. Black clusters were also visible on AO images showing white dots. These black clusters were unlikely optical artefacts because they were observed at the same location on consecutive examinations and because they were present in all examined cat eyes. On human AO images, smaller black elements were also detected and they were attributed to blood vessel crossing because blood vessels were found extending from these black elements.[30] On cat images, vessels were not observed in contact to black clusters. Therefore, it remains unclear if they represent blood vessel or instead other pigmentation as in the retinal pigment epithelium.

To the best of our knowledge, this is the first time that retinal images were obtained using AO in sedated cats. The images can be easily obtained but more research is needed to interpret them. However, the images obtained allowed us to visualize retinal cells as well as small blood vessels and nerve fiber bundles. Blood vessel walls were more sharply resolved than in conventional fundus images. AO can be an essential tool in comparative ophthalmology for both clinical and research applications.

REFERENCES

1. Wolfing JI, Chung M, Carroll J *et al.* High-resolution retinal imaging of cone-rod dystrophy. *Ophthalmology* 2006; **113**: 1014–1019.
2. Roorda A, Zhang Y, Duncan JL. High-resolution in vivo imaging of RPE Mosaic in eyes with retinal disease. *Investigative Ophthalmology and Visual Science* 2007; **48**: 2297–2303.
3. Duncan JL, Zhang Y, Ganghi J *et al.* High-resolution imaging with adaptive optics in patients with inherited retinal degeneration. *Investigative Ophthalmology and Visual Science* 2007; **48**: 3283–3291.
4. Yoon MK, Roorda A, Zhang Y *et al.* Adaptive Optics Scanning laser Ophthalmoscopy images in a family with the mitochondrial DNA T8993C mutation. *Investigative Ophthalmology and Visual Science* 2009; **50**: 18380–18470.
5. Zwick H, Lund DJ, Elliot R *et al.* Confocal spectral ophthalmoscopic imaging of retinal laser damage in small vertebrate eyes. *Proceedings of Society Photo-Optical Instruments Engineering* 1995; **2674**: 80–88.
6. Rosolen SG, Saint-Macary G, Gautier V *et al.* Ocular fundus images with confocal scanning laser ophthalmoscopy in the dog, monkey and minipig. *Veterinary Ophthalmology* 2001; **4**: 41–45.
7. Rosolen SG, Saint-Macary G, Gautier V *et al.* SLO angiography: arterio-venous filling times in monkey and minipig. *Veterinary Ophthalmology* 2002; **5**: 19–22.
8. Gekeler F, Gmeiner H, Völker M *et al.* Assessment of the posterior segment of the cat eye by optical coherence tomography (OCT). *Veterinary Ophthalmology* 2007; **10**: 173–178.
9. Hofer H, Artal P, Singer B *et al.* Dynamics of the eye's wave aberration. *Journal of Optical Society of American Association, Optics, Images, Science and Vision* 2001; **18**: 497–506.
10. Thibos LN, Bradley A, Hong X. A statistical model of aberration structure of normal, well-corrected eyes. *Ophthalmic and Physiological Optics* 2002; **22**: 427–433.
11. Liang J, Williams DR. Aberrations and retinal image quality of the normal human eye. *Journal of Optical Society of America Association, Optics, Images, Science and Vision* 1997; **14**: 2873–2883.
12. Guirao A, Porter J, Williams DR *et al.* Calculated impact of higher-order monochromatic aberrations on retinal image quality in a population of human eyes. *Journal of Optical Society of America Association, Optics, Images, Science and Vision* 2002; **19**: 620–628.
13. Tyson RK. *Principles of Adaptive Optics*, 2nd edn. Academic Press Inc., Boston 1998; 345.
14. Liang J, Grimm B, Goetz S *et al.* Objective measurement of wave aberrations of the human eye with the use of a Hartmann-Shack wavefront sensor. *Journal of Optical Society of American Association, Optics, Images, Science and Vision* 1994; **11**: 1949–1957.
15. Prieto PM, Vargas-Martin F, Goetz S *et al.* Analysis of the performance of the Hartmann-Shack sensor in the human eye. *Journal of Optical Society of American Association, Optics, Images, Science and Vision* 2000; **17**: 1388–1398.
16. Ramamirtham R, Kee C, Hung L-F *et al.* Wave aberrations in rhesus monkeys with vision-induced ametropias. *Vision Research* 2007; **47**: 2751–2766.
17. Garcia de la Cera E, Rodriguez G, Llorente L *et al.* Optical aberrations in the mouse eye. *Vision Research* 2006; **47**: 2546–2553.
18. Harmening WM, Vobig MA, Walter P *et al.* Ocular aberrations in barn owl eyes. *Vision Research* 2007; **47**: 2934–2942.
19. Bühren J, Yoon G, Kenner S *et al.* The effect of optical zone decentration on lower- and higher-order aberrations after photorefractive keratectomy in a cat model. *Investigative Ophthalmology and Visual Science* 2007; **8**: 5806–5814.
20. Huxlin KR, Yoon G, Nagy L *et al.* Monochromatic ocular wavefront aberrations in the awake-behaving cat. *Vision Research* 2004; **44**: 2159–2169.
21. Rosolen SG, Lamory B, Chateau N *et al.* Wavefront measurement aberration in dog & cat eyes. *Investigative Ophthalmology and Visual Science* 2008 [ARVO abstract no. 982].
22. Doble N, Yoon G, Chen L *et al.* Use of a microelectromechanical mirror for adaptive optics in the human eye. *Optics Letter* 2001; **27**: 1537–1539.
23. Fernandez EJ. Ultralight resolution optical coherence tomography with adaptive optics: experimental results and limits to the performance. In: *Engineering the Eye II: Imaging the Retina*. National University of Ireland, Galway, 2006; 14.
24. Glanc M, Gendron E, Lacombe F. Towards wide-field retinal imaging with adaptive optics. *Optics Communications* 2004; **230**: 225–238.
25. Paques M, Guyomard J-L, Simonutti M *et al.* Panretinal, high-resolution color photography of the mouse fundus. *Investigative Ophthalmology and Visual Science* 2007; **48**: 2769–2774.

26. Guyomard J-L, Rosolen SG, Paques M *et al.* A low-cost and simple imaging technique of the anterior and posterior segments: eye fundus, ciliary bodies, iridocorneal angle. *Investigative Ophthalmology and Visual Science* 2008; **49**: 5168–5174.
27. Rosolen SG, Rigaudière F, LeGargasson J-F *et al.* Recommendations for a toxicological screening ERG procedure in laboratory animals. *Documenta Ophthalmologica* 2005; **110**: 57–66.
28. Rosolen SG, Rigaudière F, Lachapelle P. A practical method to obtain reproducible binocular electroretinograms in dogs. *Documenta Ophthalmologica* 2002; **105**: 93–103.
29. Samuelson DA. Ophthalmic anatomy. In: *Veterinary Ophthalmology*, 4th edn. (ed. Gelatt KN) Blackwell Publishing, Iowa, IA, 2007; 37–148.
30. Nakashima K, Roche O, Massamba N *et al.* Assessment of cone mosaic imaging performance using flood-illumination adaptive optics in ametropia. *Investigative Ophthalmology and Visual Science* 2009 [ARVO abstract no. 1066].
31. Steinberg RH, Reid M, Lacy PL. The distribution of rods and cones in the retina of the cat. *Journal of Comparative Neurology* 1973; **148**: 229–235.
32. Linberg KA, Lewis GP, Shaaw C *et al.* Distribution of S- and M-cones in normal and experimentally detached cat retina. *Journal of Comparative Neurology* 2001; **430**: 343–356.
33. Casteron-Mochon JF, Lopez-Gil N, Benito A *et al.* Ocular wavefront aberration statistics in a normal young population. *Vision Research* 2002; **42**: 1611–1617.
34. Thibos LN, Hong X, Bradley A *et al.* Statistical variation of aberration structure and image quality in a normal population of healthy eyes. *Journal of Optical Society of American Association, Optics, Images, Science and Vision* 2002; **19**: 2329–2348.
35. Koh S, Maeda N, Kuroda T *et al.* Effect of tear film break-up on higher-order aberrations measured with wavefront sensor. *American Journal of Ophthalmology* 2002; **134**: 115–117.
36. Kufoy EA, Pakalnis VA, Parks CD *et al.* Keratoconjunctivitis sicca associated secondary uveitis elicited in rats after systemic xylazine/ketamine anesthesia. *Experimental Eye Research* 1989; **49**: 861–871.
37. Tita B, Leone MG, Casini ML *et al.* Corneal toxicity of xylazine and clonidine, in combination with ketamine, in the rat. *Ophthalmic Research* 2001; **33**: 345–352.